Catalytic Coupling of Free Radical Oxidation and Electrophilic Chlorine Addition by Phase-transfer Intermediates in Liquid Aerosols

Authors: Meirong Zeng,[1,#] Chen-Lin Liu,[2] Kevin R. Wilson[1,*]

Affiliations:

[1]Chemical Sciences Division, Lawrence Berkeley National Laboratory, Berkeley, CA 94720, USA.

[2]Scientific Research Division, National Synchrotron Radiation Research Center, Hsinchu 30076, Taiwan

[#]Current Address: College of Smart Energy, Shanghai Jiao Tong University, Shanghai, 200240

***Corresponding author**: Kevin R. Wilson (email: krwilson@lbl.gov, Phone: 510-495-2474)

ORCID: Kevin R. Wilson, 0000-0003-0264-0872

Meirong Zeng, 0000-0003-3902-7430

Keywords

Electrophilic addition, free radical chemistry, heterogeneous olefin chlorination, phase-transfer catalyst, biphasic catalysis

Abstract

While examining the heterogeneous reaction of chlorine atoms with alkenes, in the presence of Cl_2, we have observed an unexpectedly large enhancement of reactivity and the predominance of chlorinated reaction products even under high O_2 conditions, where Cl atom recycling is expected to be minimal. These observations cannot be explained by known free radical oxidation or cycling mechanisms, but rather we find evidence for the multiphase catalytic coupling of free radical oxidation with electrophilic Cl_2 addition. The mechanism entails the production of oxygenated reaction intermediates, which act as gas-liquid phase transfer catalysts (gl-PTC) by promoting the accommodation of gas phase Cl_2 by the aerosol; thereby enhancing electrophilic addition. Although, the majority of PTC typically couple chemistry between two immiscible liquid phases (aqueous/organic), there are few examples of PTC that couple gas-liquid reactions. This work shows how multiphase reaction schemes of aerosols can be reimagined for understanding catalytic reaction mechanisms.

Introduction

Phase transfer catalysts (PTC) chaperone reagents between phases to promote a reaction[1-3]. Most common are PTC that transport reactants across liquid-liquid interfaces[3] to improve reaction kinetics and selectivity. These include metals[3], salts[1-2], or crown ethers[4-6]. Much less common are gas-liquid phase transfer catalysts (gl-PTC) despite some clear advantages (*i.e.* no solvent) for industrial scale processes.[7] In these more conventional systems a high temperature packed bed reactor is typically combined with a gas feed and a molten phase-transfer catalyst supported on a solid substrate.[7-10]

Although, aerosol techniques are commonly used to synthesize[11-13] high surface area, porous substrates for gas-solid conversions, there are few examples, if any, of using liquid aerosols for coupling gas-liquid catalytic reactions. In contrast there are a number of studies that show homogeneous catalytic pathways occurring inside aqueous aerosol analogs, where catalytic transformations are driven by transition metals or ammonium salts.[14-17] Here we report evidence for the catalytic coupling of free radical oxidation and electrophilic Cl_2 addition in room temperature liquid organic aerosols, which is mediated by the production of oxygenated molecules that act as gl-PTC. To our knowledge, this is a unique example of a gl-PTC operating at room temperature. This builds upon our previous work[18] where we focused solely on how the Cl_2 heterogeneous addition rate is altered by the presence of molecules doped into alkene droplets.

Previously we showed that the rate of heterogeneous addition of gas phase Cl_2 to liquid squalene (Sqe, $C_{30}H_{50}$, a branched alkene), in submicron aerosol particles, could be catalytically enhanced by the addition of oxygenated molecules to the liquid or gas phases[18]. For example, although 2-decyl-1-tetradecanol ($C_{24}OH$, $C_{24}H_{50}O$, a branched alcohol) did not alter the distribution of reaction products, its presence inside the aerosol accelerated (up to ~ 20×) the

electrophilic addition of Cl_2 to the alkene, as shown in Fig. S1 in the Supporting Information. Prior literature on the surface partitioning of oxygenated molecules in organic solvents and additional experimental evidence presented in Ref.[18], suggest that the presence of oxygenates enhances the aerosol capture of Cl_2 gas, likely by prolonging its lifetime at the gas-aerosol interface. This in turn promoted faster solvation and electrophilic Cl_2 addition to the alkene. In the case of the gas-phase oxygenated additives, it is proposed that they adsorb to the aerosol surface to further enhance Cl_2 capture by the particles. Although further theoretical support is needed, we hypothesized that weak interfacial halogen-bonds between adsorbed Cl_2 and the oxygenated additives were responsible for the enhanced capture of Cl_2 by the aerosols. These previous observations[18] motivated us to explore, using aerosols, the coupling of free radical oxidation with electrophilic addition, since free radical oxidation produces many of the same kinds of oxygenated reaction products (*i.e.* ketones and alcohols) that we previously found to be effective gl-PTC for the electrophilic Cl_2 addition to olefins.

Experimental Methods

An aerosol flow tube and continuous flow stirred tank reactor (CFSTR) are used in this study. Both of these setups have been widely used to explore heterogeneous reactions of aerosols with ozone[19], hydroxyl radical[20], iodine[21], and chlorine[22]. Additional technical details about the reactors can be found elsewhere.[23-25] Here we briefly review key experimental details.

The flow tube reactor (140 cm long and 2.5 cm inner diameter, 0.7 Liter) has an average reaction time of 37 seconds compared to the CFSTR (volume = 147 Liter), which has reaction times of hours and operates at much lower reagent concentrations. Both reactors are equipped with

UV lamps (blacklights, λ ~ 356 nm) to photolyze Cl_2 gas to produce Cl atoms *in situ*. Both reactors were operated at a total flow of 1.1 SLM at room temperature and pressure.

Aerosols are homogeneously nucleated by passing 300 SCCM N_2 through a heated Pyrex tube that contains the organic liquid, *e.g.* Sqe, linolenic acid (LNA) and oleic acid (OA) (purchased from Sigma-Aldrich). The Pyrex tube is placed inside a tube furnace to control the temperature of the liquid. A scanning mobility particle sizer (SMPS, TSI) is used to monitor the particle concentration and diameter, which remain invariant during the reaction. Aerosols nucleate in a log-normal distributed with the average concentration of ~ 10^6 cm^{-3} and mean diameter of ~ 200 nm. The particle-laden flow is then passed through an annular activated charcoal denuder to remove any residual gas phase organics produced in the furnace. Prior to entering the reactor, the particle flow is mixed with additional flows of Cl_2, O_2, N_2 and a gas phase tracer. The final [Cl_2] in the reactor is achieved by diluting flow from a standard cylinder (54.6 ppm Cl_2 balanced with N_2, purchased from Praxair) with N_2.

The [Cl] is controlled by adjusting the power to the UV lamps using a Variac. A gas phase tracer (*e.g. n*-hexane or 2-methyl-2-butene) is added at ~ 200 ppb in order to determine the [Cl], using a relative rate technique described elsewhere.[22, 25] A gas chromatograph with a flame ionization detector is utilized to record the decay of the gas phase tracer to determine the [Cl] exposure in the reactor. Additional checks with and without the tracer show that it does not alter the overall chemistry.

The reactive decay of Sqe, LNA, or OA is measured using a vacuum ultraviolet aerosol mass spectrometer (VUV-AMS).[20, 22, 24] To record mass spectra, the aerosol is first vaporized at ~ 125 ºC and then photoionized by the VUV light at 9.6 eV for Sqe. The decay kinetics are quantified

as a function of [Cl_2], [O_2] and [Cl]. Since Cl_2 reacts slowly with the alkenes in the dark, via electrophilic Cl_2 addition,[18] experiments are conducted by fixing the [Cl_2] in the reactor and first measuring the amount of the alkene consumed in the dark (*i.e.* without Cl atoms). In the flow tube reactor, this baseline dark reaction scales linearly with [Cl_2] and reduces the alkene signal by 5% at [Cl_2] ~ 1 ppm and 18% at [Cl_2] = 4 ppm as shown in Fig. S4. The UV lights are then turned on to initiate the Cl atom reaction. The [Cl] in the reactor is changed by increasing the photon flux of the lamps. γ_{eff} is then computed from the decay kinetics (Fig. S5) in the presence of light, the [Cl] or exposure ([Cl] × time), and the gas-surface collision frequency obtained from gas kinetic theory.

To more easily observe the reaction products, difference mass spectra (reacted Sqe spectra – unreacted Sqe spectrum) are reported throughout the manuscript. Product intensities are reported relative to unreacted Sqe (*e.g.* [SqeCl]/[Sqe]$_0$) instead of absolute concentrations, due to the lack of authentic standards needed to determine absolute photoionization cross-sections and ion fragmentation probabilities.[22-25] The formulas and *m/z* of reactants and products discussed in this work can be found in Table S1.

Results and Discussion

For the experiments described below, we make extensive use of effective reaction probabilities (γ_{eff}) to interpret our results. γ_{eff} is a measure of consumption rate of a species within the aerosol relative to the collision frequency of a gas phase molecule. Here the gas-surface collision frequency of Cl atoms is used as a clock for measuring the relative reaction rate. If the rate of decay of a molecule in the aerosol proceeds at or near the collision rate, then γ_{eff} = 1. Alternatively, if the reaction is inefficient, as in the case of electrophilic addition of Cl_2, then the consumption rate of the alkene relative to the Cl_2 gas collision rate is much less than 1 (*i.e.* γ_{eff} ~

3.5×10^{-5}, see Ref.[18]). There are examples[20, 22, 26-27] where $\gamma_{eff} > 1$, which indicate the influence of secondary reactions (*i.e.* radical chain reactions) that consume the particle phase species at rates that can exceed the collision frequency of the gas phase reactant.

An example of a system that shows $\gamma_{eff} > 1$, which provides context for this work, is the previously published study[22] involving the Cl atom initiated heterogeneous free radical oxidation of squalane (Sqa, $C_{30}H_{62}$, a branched alkane). As previously reported by Liu *et al.*[22] and shown in

Fig. 1A, γ_{eff} exceeds 1, in the absence of O_2, and is observed to increase as [Cl_2] is elevated in the reactor. As the fraction of O_2 in the reaction mixture approaches ~ 0% in Fig. 1B (balance is N_2

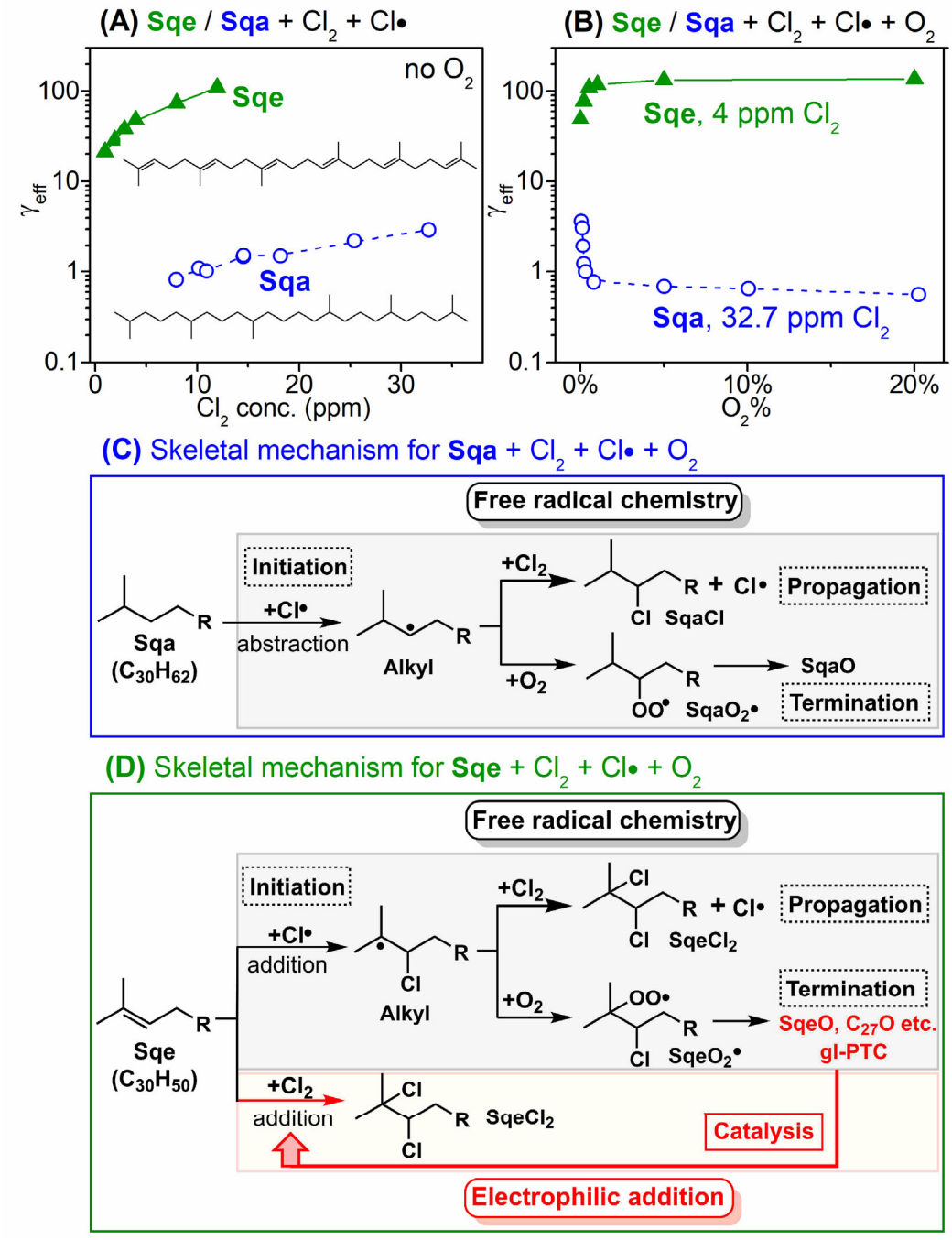

Fig. 1. Effective reaction probabilities (γ_{eff}) and reaction scheme. (A) γ_{eff} of Sqe and Sqa as a function of [Cl_2]. (B) γ_{eff} of Sqe and Sqa as a function of [O_2]. (C) A skeletal reaction mechanism for Sqa, which only includes free radical chemistry. (D) A skeletal reaction mechanism for Sqe, which includes both free radical chemistry and electrophilic addition.

with trace Cl_2), $\gamma_{eff} \sim 3.6$, indicating that for every Cl collision with the aerosol surface, at least 3.6 molecules of Sqa are consumed. Liu *et al.* further observed a rapid decrease in γ_{eff} with increasing $[O_2]$ as is shown in Fig. 1B. With increasing O_2, γ_{eff} decreases approaching an asymptotic value of ~ 0.5 when 20% of the reaction flow is oxygen (*i.e.* $[O_2] = 20\%$). These changes in heterogeneous reaction rate as a function of $[O_2]$ and $[Cl_2]$, are accompanied by a change in the reaction products; from chlorinated alkanes at low O_2 to ketones and alcohols at high O_2 as shown in Fig. S2.

As illustrated in Figs. 1C and S2-S3, these changes in reaction rate and product distributions are consistent with the well-known competition between Cl_2 and O_2 for the reaction with the alkyl radicals (R·) that are formed via H atom abstraction by Cl atoms. The $R\cdot + Cl_2$ reaction forms chlorinated products, whereas the $R\cdot + O_2$ produces peroxy radicals ($RO_2\cdot$) that undergo self-reactions (*i.e.* $RO_2\cdot + RO_2\cdot$) to form stable chain terminating ketone and alcohol products (*e.g.* SqaO shown in Figs. 1C, S2-S3). Cl atoms are a co-product of the chlorinated alkanes (*e.g.* SqaCl) that are formed by the $R\cdot + Cl_2$ step, which is favored in the absence of O_2. This additional population of Cl atoms can go on to further attack Sqa in chain reactions, which explains why γ_{eff} is larger than 1. These prior results will aid in interpreting the catalytic coupling mechanism described below.

A series of experiments are designed to explore the heterogeneous reactivity of Cl atoms, in the presence of O_2 and Cl_2, with a series of unsaturated molecules. Sqe, LNA and OA are selected as model systems and differ in the number of C=C bonds and overall molecular structure. These molecules are also key components of skin lipids,[28] which act as a barrier against environmental chemical exposure. The heterogeneous reactions are studied in a flow tube and

CFSTR enabling access to a broad range of reaction timescales, concentrations of gas phase Cl atoms and Cl_2.

As shown for Sqe in Fig. 1A, γ_{eff}, in the absence of $[O_2]$ is observed to increase with $[Cl_2]$. The observed decay kinetics of Sqe vs. [Cl] and $[Cl_2]$ that are used to compute γ_{eff} are shown in Fig. S5. At $[Cl_2] \sim 1$ ppm, $\gamma_{eff} = 20$ and approaches a value of 100 at $[Cl_2] > 10$ ppm. This trend provides clear evidence for secondary reactions propagated by Cl atoms as shown in Figs. 1D and S6. Values of γ_{eff} in large excess of 1 are consistent with chain reactions, which, as is discussed above, are consistent with Cl atom recycling in the $R\cdot + Cl_2 \rightarrow RCl + Cl\cdot$ pathway. This mechanism is similar to the one described above and shown in Fig. 1C for Sqa. The major difference between the two pathways (Sqe vs. Sqa) arises from the presence of C=C bonds, which in Sqe favor Cl atom addition rather than H-atom abstraction.[29] As shown in Fig. S7, additional experiments are performed without O_2 in the CFSTR over reaction times of hours at much lower concentrations ($[Cl_2] \sim 300$ ppb and $[Cl] \sim 10^5$ molecules$\cdot$cm^{-3}). The increase in γ_{eff} with $[Cl_2]$ is qualitatively consistent with the trend shown in Fig. 1A and further show, as expected, that there is substantial chain chemistry in the absence of O_2, the magnitude of which scales with $[Cl_2]$.

Shown in Figs. 1B and S8 are the changes in γ_{eff} when O_2 is added to the flow tube reactor. Unexpectedly, the behavior of γ_{eff} vs. $[O_2]$ for Sqe is exactly opposite from what was previously

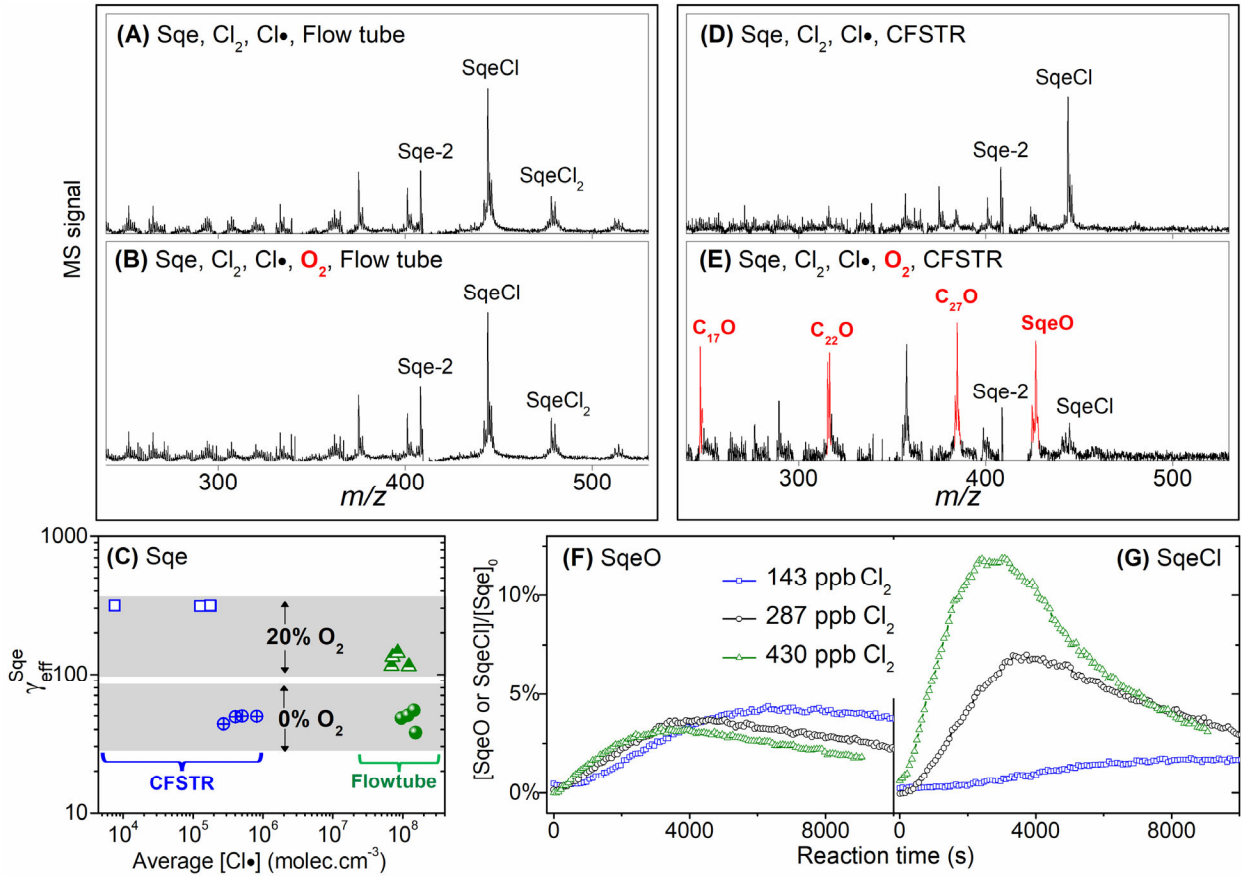

Fig. 2. Difference mass spectra, γ_{eff} and heterogeneous reaction kinetics. Difference mass spectra for the Sqe reaction obtained in the flow tube reactor (A) without O_2 and (B) with 20% O_2. Difference mass spectra for the Sqe reaction obtained in the CFSTR (D) without O_2 and (E) with 20% O_2. (C) Compiled values for γ_{eff} as a function of $[O_2]$, [Cl] and $[Cl_2]$ obtained in flow tube and CFSTR reactors. (F and G) Formation kinetics of oxygenated (SqeO) and chlorinated products (SqeCl) as a function of reaction time in CFSTR (with $[O_2]$ = 20%).

observed for Sqa. Similar behavior is observed for LNA and OA as shown in Section S4 (Figs. S10-S12) and Section S5 (Figs. S13-S15), respectively. Rather than decreasing, γ_{eff} steeply increases with increasing O_2; reaching values in excess of 100 at $[O_2]$ = 20%. Furthermore, the observed product distribution (Figs. 2A and 2B) are exclusively chlorinated molecules (*i.e.* $SqeCl_n$) even at 20% O_2, which is also not the case for Sqa as shown in Fig. S2 (*e.g.* SqaCl and SqaO).

Although, Figs. 2A and B focus on earlier product generations, *e.g.* SqeCl and $SqeCl_2$, as the sequential reaction progresses additional product generations ($SqeCl_n$) are formed such as $SqeCl_3$, $SqeCl_4$, $SqeCl_5$. Together these observations are inconsistent with the expectation that O_2 should quench the $R\cdot + Cl_2 \rightarrow RCl + Cl\cdot$ chain reaction by forming terminal products arising from peroxy radicals ($R\cdot + O_2 \rightarrow RO_2\cdot$) self-reactions. $RO_2\cdot + RO_2\cdot$ pathways produce alcohols (ROH) and/or ketones (RC=O) via the well-known Bennett-Summers[30] ($2RO_2\cdot = 2RC{=}O + H_2O_2$) or Russell mechanisms[31] ($2RO_2\cdot = ROH + RC{=}O + O_2$).

In addition to these reactions, we considered the possible role that O_2 might play in unimolecular pathways that could lead to chain propagation. In aqueous systems the unimolecular decomposition of an α-hydroxyperoxy radical produces HO_2, which can propagate reactivity. By analogy, we considered the unimolecular decomposition of the α-chloroperoxy radical (Fig. 1D), which could in principle decompose to produce a ClO radical rather than HO_2. However, this possible propagation pathway can't explain the observed increase in γ_{eff} with increasing $[O_2]$, since the reaction of ClO with alkenes is several orders of magnitude slower than Cl atoms.[32-33] As such, this pathway would decrease the global reactivity with increasing O_2. Thus the key difference between the alkene and alkane reactions is not the free radical pathways but rather in the ability for gas Cl_2 to electrophilically add to the C=C bonds, as will be discussed below.

To further elucidate the unexpected behavior shown Figs. 1B and 2B, additional experiments are conducted in the CFSTR. Reactions conditions in the CFSTR are designed to slow down the reaction kinetics relative to the flow tube reactor where much higher [Cl] and $[Cl_2]$ and shorter reaction times (~ 37 seconds) are used. This is achieved in the CFSTR by reducing $[Cl_2]$ to ~ 100 ppb and [Cl] to 10^4-10^5 molecules·cm^{-3}. This lengthens the reaction time to hours. In the

CFSTR, γ_{eff} behaves in an analogous way as the flow tube where O_2 accelerates the reaction. Figure 2C summarizes the kinetic behavior observed in both the CFSTR and flow tube reactors. In each case, the presence of O_2 greatly accelerates the apparent reaction rate, with the magnitude of this acceleration (*i.e.* γ_{eff}) being the largest at low Cl atom densities ([Cl] = 10^4 molecules·cm^{-3}).

Similar to the results obtained in the flow tube reactor without O_2, the observed reaction products in the CFSTR at 0% O_2 are all chlorinated (*i.e.* SqeCl$_n$) as shown in Fig. 2D. However, unlike the flow tube, when [O_2] = 20%, oxygenated products are detected in the mass spectra as shown in Fig. 2E. This is explained by the large reduction in the speed of the reaction under CFSTR conditions, which lengthens the lifetime and increases the steady state concentration of these oxygenates. In contrast, under flow tube conditions, where the reaction rate is comparably fast, the oxygenates once formed are rapidly consumed, by electrophilic addition to their remaining C=C bonds, before they can be detected via mass spectrometry.

These oxygenated products are explained, in Fig. 1D, by the self-reaction of two chlorinated peroxy radicals ($C_{30}H_{50}ClO_2$), which upon disproportionation produce ketones ($C_{30}H_{49}ClO$) and alcohols ($C_{30}H_{51}ClO$) as illustrated in Fig. S6. These ketone and alcohol products are detected in the mass spectrum (labelled as SqeO in Fig. 2E and Table S1) as fragments, arising from the dissociative photoionization and the elimination of –HCl, which produces ion fragments at a mass-to-charge ratio (*m/z*) corresponding to $C_{30}H_{48}O$ (*m/z* = 424) and $C_{30}H_{50}O$ (*m/z* = 426), respectively. Similar fragmentation patterns are also observed for LNA and OA (Figs. S10-S15 and Table S1), and is a common occurrence during ionization of halogenated hydrocarbons, as observed in previous studies.[18, 21-22] Smaller molecular weight aldehydes are also observed and detected at $C_{17}H_{28}O$ (*m/z* = 248), $C_{22}H_{36}O$ (*m/z* = 316) and $C_{27}H_{44}O$ (*m/z* = 384) as shown in Fig.

2E and Table S1. These aldehydes are explained by the formation (*i.e.* $RO_2\cdot + RO_2\cdot \rightarrow 2\ RO\cdot + O_2$) and subsequent decomposition of alkoxy radicals (RO·) as shown in Fig. S6.

Figs. 2F and 2G show the kinetic evolution of the SqeO and SqeCl products in the CFSTR. The relative intensity of SqeO is larger than SqeCl only when the $[Cl_2]$ is very low (*e.g.* 143 ppb). As $[Cl_2]$ increases to 430 ppb, the intensity of SqeO decreases relative to SqeCl. These results show that there is a relatively narrow range in $[Cl_2]$ where oxygenated products, in the presence of 20% O_2, can be observed and their intensity is comparable to or larger than that of their chlorinated analogs. These results confirm that Cl atom-initiated oxidation is in fact occurring in this system, although the dramatic acceleration in apparent reaction rate and the dominance of purely chlorinated reactions products with increasing $[O_2]$ is not consistent with known radical reaction mechanisms.

In the absence of O_2, the alkyl radicals (R·), formed either by H-abstraction in Sqa or abstraction/addition in the case of Sqe, react with Cl_2 to form chlorinated products and a Cl atom co-product. This leads, in both cases, to $\gamma_{eff} > 1$, the magnitude of which scales $[Cl_2]$. The absolute magnitude of γ_{eff} for Sqe is larger than Sqa and presumably reflects the faster reaction rate of Cl with alkenes[29] vs. alkanes[34]. In both cases, chlorinated products are formed.

However, in the presence of $[O_2]$, γ_{eff} for Sqa and Sqe follow dramatically different and opposite trends. For Sqa, the behavior is consistent with the formation of chain terminating peroxy radicals (Fig. 1C), which extinguish the $R\cdot + Cl_2$ propagation pathway and reduce γ_{eff} to values less than 1. As shown by Liu *et al.*,[22] the functional form of γ_{eff} vs. $[O_2]$ for Sqa as shown in Fig. 1B simply reflects the differences in the rate of reaction of R· with O_2 and Cl_2. This is determined by the difference in bimolecular rate coefficients (k) for the $R\cdot + Cl_2$ and $R\cdot + O_2$ reactions (which

differ by a factor of ~ 20 [22, 35]), as well as the Henry's law solubility (H) of Cl_2 and O_2 in the aerosol. Cl_2 gas is estimated to be ~ 60 times more soluble than O_2 in hydrocarbons.[36-38] Thus the $R\cdot + Cl_2$ rate is expected to be ~ 1200 times faster than $R\cdot + O_2$ for the case where $[Cl_2] = [O_2]$. However, under the experimental conditions reported here and in Liu *et al.*,[22] there is ~ 2000 times more gas phase O_2 than Cl_2 in the reactor, which explains the steep decrease in γ_{eff} vs. $[O_2]$ observed for Sqa and shown in Fig. 1B.

The Henry's law solubility of Cl_2 in Sqe is not expected to be all that different from Sqa or other hydrocarbons.[37] Furthermore, in the gas phase, the rate coefficient for O_2 addition to an alkyl radical is not expected to change by orders of magnitude with varying molecular structure.[39-40] As such, these factors are insufficient to explain why γ_{eff} for Sqe increases with $[O_2]$. Instead, these results can be explained by the acceleration of electrophilic Cl_2 addition, which is catalytically coupled to free radical oxidation through the production of the oxygenated intermediates, which act as the gas-liquid phase transfer catalysts (gl-PTC), as shown schematically in Fig. 3 and discussed below.

Previously we showed that the rate of electrophilic Cl_2 addition to Sqe could be modulated by the adding spectator molecules to either the gas or aerosol phases.[18] The electrophilic addition rate to Sqe could be accelerated by up to 20× in the presence of molecules containing oxygenated

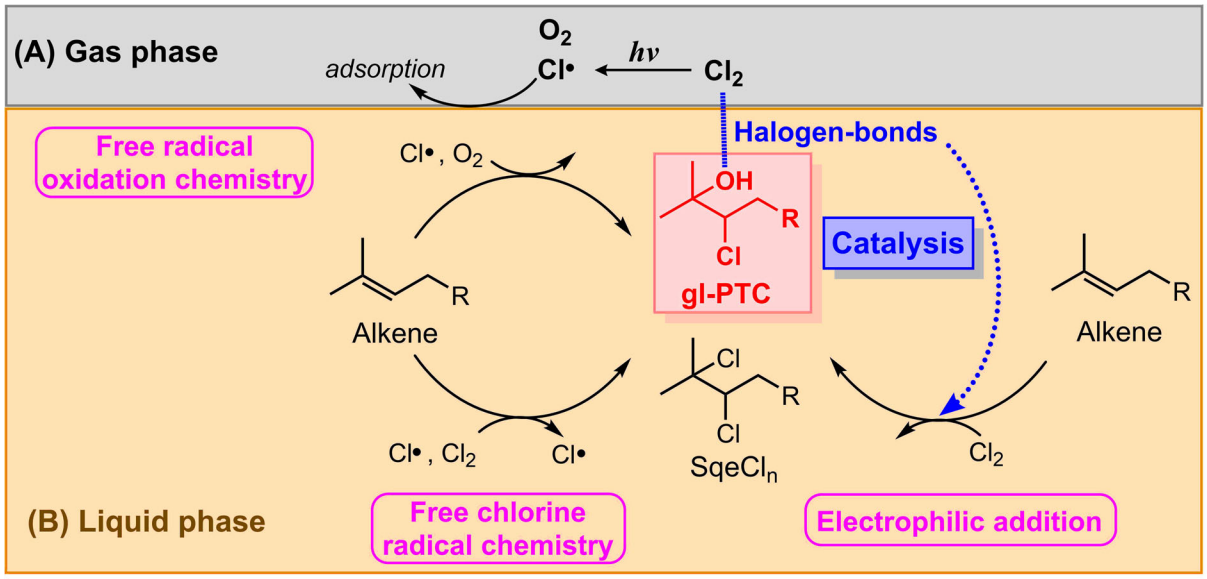

Fig. 3. Reaction scheme showing the catalytic coupling of electrophilic addition and free radical oxidation. (A) Gas phase species include O_2, Cl_2 and Cl atoms, produced by the UV photolysis of Cl_2 gas. These species collide and adsorb onto the surface of aerosol containing alkenes. (B) The liquid phase contains an alkene. Reactions with adsorbed Cl_2, Cl and O_2, produce chlorinated ($SqeCl_n$) and oxygenated products (gl-PTC). gl-PTC are produced by free radical oxidation pathways, which in turn promote Cl_2 accommodation to the aerosol and it subsequent electrophilic addition to the alkene.

functional groups as shown in Fig. S1. Although, Cl_2 addition to pure Sqe is measured to be a minor loss channel prior to free radical oxidation, accounting for the consumption of only 5-18% of the alkene, as shown in Fig. S4, if the electrophilic addition rate were to increase by 10×, it would then, in fact, dominate the chemistry. This could occur since as free radical oxidation forms oxygenated products (*e.g.* ketones, alcohols and aldehydes) as shown in Figs. 2E and 2F. These products in turn catalyze the electrophilic addition as shown in Fig. 3. Under these conditions, γ_{eff} would appear to increase since it is computed relative to the Cl atom collision frequency and not using [Cl_2] gas, which controls the electrophilic addition rate. Furthermore, electrophilic addition

produces exclusively chlorinated reaction products and explains why, despite high [O_2] in the reactor, only chlorinated products are observed. This also explains why Sqa and Sqe exhibit such different behaviors towards [O_2], since electrophilic addition requires the presence of C=C bonds.

From our previous studies[18], we concluded that oxygenated aerosol additives (*i.e.* species with alcohol and acid functional groups) act as gl-PTC that promote the accommodation of Cl_2 gas by the aerosol. We hypothesized that the mechanism for the enhanced accommodation involved the slowing of the Cl_2 desorption kinetics from the aerosol surface. Although further theoretical support is needed, it appears that weak interactions (*i.e.* halogen-bonding) between oxygenated functional groups and adsorbed Cl_2 were responsible for the slower desorption kinetics. Slower desorption kinetics favor solvation (*i.e.* phase transfer) of gas phase Cl_2 and its subsequent reaction in the aerosol. It is likely that a similar catalytic mechanism is operating here: free radical oxidation produces oxygenated molecules *in-situ* (*i.e.* gl-PTC) that enhance Cl_2 gas capture, catalyzing the subsequent electrophilic addition to Sqe as illustrated in Fig. 3.

Conclusions

Here we report evidence for the accelerated heterogeneous reactivity of liquid aerosols that can be explained by a catalytic mechanism involving the transient production of gl-PTC. Although we have provided a reasonable hypothesis to explain our experimental results, there is a clear need for a detailed molecular-level understanding of possible catalytic mechanisms. For example, ascertaining how the presence of oxygenates either enhances the accommodation of Cl_2 into the aerosol or directly catalyze the electrophilic addition reaction remain open questions. Previous theoretical work on halogen bonding indicate it can play a significant role for reactions at liquid water surfaces.[41] Similar theoretical work might be needed here to identify whether halogen

bonding occurs at the interface and whether it is significant enough to alter the residence time of Cl_2 on the surface. Molecular dynamics (MD) simulations could be employed to compute free energy profiles for the transfer of gas phase Cl_2 into liquid Sqe with and without the presence of gl-PTC. Such molecular level information would be required to construct a physically realistic kinetic model that includes the elementary steps of Cl_2 adsorption, desorption, solvation and reaction. Experimentally, molecular beam scattering experiments could be useful in understanding how oxygenates at the surface of Sqe might alter the desorption dynamics of Cl_2. Surface sensitive spectroscopies might be used to understand the degree to which oxygenated solutes partition to the interface of Sqe.

In conclusion, this work suggests that submicron liquid particles suspended in a gas could be a useful system to examine gas-liquid catalysis. Due to their small size, aerosols have several useful advantages over macroscale reactors for gas-liquid heterogeneous conversions, such as faster liquid phase diffusion and gas-liquid equilibration times. Aerosol-sized containers also have a much larger fraction of molecules residing at the interface compared to macroscale reaction vessels. Furthermore, weak interactions at the gas-liquid interface can have substantial effects on mass transfer of gas into aerosols, which provides additional options for designing aerosol systems for catalytic transformations. These results, in addition to others in the literature,[11, 14-17] show how the multiphase chemistry of aerosols can be employed to study catalytic reactions beyond their more typically application in atmospheric chemistry.

Supporting Information

Supporting information that is available:

Table S1. The formulas and *m/z* of reactants and products discussed in this work.

Section S1. Reference observations for Sqe + Cl_2 + gl-PTC additives reactions

Section S2. Reference observations for Sqa (no C=C) + Cl_2 + Cl atom

Section S3. Additional experiments for Sqe (6 C=C) + Cl_2 + Cl atom

Section S4. Additional experiments for LNA (3 C=C) + Cl_2 + Cl atom

Section S5. Additional experiments for OA (1 C=C) + Cl_2 + Cl atom

Acknowledgment

We thank Bruce Rude for assistance at the ALS, Musahid Ahmed, Martin Head-Gordon and Jonathan Wong for helpful discussions. This work was supported by Gas Phase Chemical Physics program in the Chemical Sciences Geosciences and Biosciences Division of the Office of Basic Energy Sciences of the U.S. Department of Energy under Contract No. DE-AC02-05CH11231. This research used resources of the Advanced Light Source, which is a U.S. Department of Energy Scientific User Facility under contract no. DE-AC02-05CH11231.

Competing interests

The authors declare no conflict of interest.

References

(1) Pupo, G.; Ibba, F.; Ascough, D. M. H.; Vicini, A. C.; Ricci, P.; Christensen, K. E.; Pfeifer, L.; Morphy, J. R.; Brown, J. M.; Paton, R. S., et al. Asymmetric Nucleophilic Fluorination under Hydrogen Bonding Phase-Transfer Catalysis. *Science* **2018**, *360*, 638–642.

(2) Patel, N.; Sood, R.; Bharatam, P. V. NL_2^+ Systems as New-Generation Phase-Transfer Catalysts. *Chem. Rev.* **2018**, *118*, 8770–8785.

(3) Crossley, S.; Faria, J.; Shen, M.; Resasco, D. E. Solid Nanoparticles That Catalyze Biofuel Upgrade Reactions at the Water/Oil Interface. *Science* **2010**, *327*, 68–72.

(4) Ooi, T.; Maruoka, K. Recent Advances in Asymmetric Phase-Transfer Catalysis. *Angew. Chem. Int. Ed.* **2007**, *46*, 4222–4266.

(5) Dehmlow, E. V. Advances in Phase-Transfer Catalysis [New Synthetic Methods (20)]. *Angew. Chem. Int. Ed. Engl.* **1977**, *16*, 493–505.

(6) Stott, P. E.; Bradshaw, J. S.; Parish, W. W. Modified Crown Ether Catalysts. 3. Structural Parameters Affecting Phase Transfer Catalysis by Crown Ethers and a Comparison of the Effectiveness of Crown Ethers to That of Other Phase Transfer Catalysts. *J. Am. Chem. Soc.* **1980**, *102*, 4810–4815.

(7) Tundo, P.; Moraglio, G.; Trotta, F. Gas-Liquid Phase-Transfer Catalysis: A New Continuous-Flow Method in Organic Synthesis. *Ind. Eng. Chem. Res.* **1989**, *28*, 881–890.

(8) Angeletti, E.; Tundo, P.; Venturello, P. Gas-Liquid Phase-Transfer Catalysis: Wittig-Horner Reaction in Heterogeneous Conditions. *J. Chem. Soc. Perkin Trans.* **1987**, *1*, 713–714.

(9) Totten, G. E.; Clinton, N. A. Poly(Ethylene Glycol) and Derivatives as Phase Transfer Catalysts. *J. Macromol. Sci., Part C: Polymer Reviews* **1998**, *38*, 77–142.

(10) Mathias, L. J.; Charles E. Carraher, J. *Crown Ethers and Phase Transfer Catalysis in Polymer Science*; Springer: Boston, MA, 1984; Vol. 23, pp 275–290.

(11) Debecker, D. P.; Bras, S. L.; Boissière, C.; Chaumonnot, A.; Sanchez, C. Aerosol Processing: A Wind of Innovation in the Field of Advanced Heterogeneous Catalysts. *Chem. Soc. Rev.* **2018**, *47*, 4112–4155.
(12) Weber, A. P.; Seipenbusch, M.; Kasper, G. Application of Aerosol Techniques to Study the Catalytic Formation of Methane on Gasborne Nickel Nanoparticles. *J. Phys. Chem. A* **2001**, *105*, 8958–8963.
(13) Gradon, L.; Balgis, R.; Hirano, T.; Rahmatika, A. M.; Ogi, T.; Okuyama, K. Advanced Aerosol Technologies towards Structure and Morphologically Controlled Next-Generation Catalytic Materials. *J. Aerosol Sci.* **2020**, *149*, 105608.
(14) Nozière, B.; Dziedzic, P.; Córdova, A. Inorganic Ammonium Salts and Carbonate Salts Are Efficient Catalysts for Aldol Condensation in Atmospheric Aerosols. *Phys. Chem. Chem. Phys.* **2010**, *12*, 3864–3872.
(15) Nozière, B.; Fache, F.; Maxut, A.; Fenet, B.; Baudouin, A.; Fine, L.; Ferronato, C. The Hydrolysis of Epoxides Catalyzed by Inorganic Ammonium Salts in Water: Kinetic Evidence for Hydrogen Bond Catalysis. *Phys. Chem. Chem. Phys.* **2018**, *20*, 1583–1590.
(16) Wang, W.; Liu, M.; Wang, T.; Song, Y.; Zhou, L.; Cao, J.; Hu, J.; Tang, G.; Chen, Z.; Li, Z., et al. Sulfate Formation Is Dominated by Manganese-Catalyzed Oxidation of SO_2 on Aerosol Surfaces During Haze Events. *Nat. Commun.* **2021**, *12*, 1993.
(17) Jang, M.; Czoschke, N. M.; Lee, S.; Kamens, R. M. Heterogeneous Atmospheric Aerosol Production by Acid-Catalyzed Particle-Phase Reactions. *Science* **2002**, *298*, 814–817.
(18) Zeng, M.; Wilson, K. R. Experimental Evidence That Halogen Bonding Catalyzes the Heterogeneous Chlorination of Alkenes in Submicron Liquid Droplets. *Chem. Sci.* **2021**, *12*, 10455–10466.
(19) Heine, N.; Houle, F. A.; Wilson, K. R. Connecting the Elementary Reaction Pathways of Criegee Intermediates to the Chemical Erosion of Squalene Interfaces During Ozonolysis. *Environ. Sci. Technol.* **2017**, *51*, 13740–13748.
(20) Zeng, M.; Heine, N.; Wilson, K. R. Evidence That Criegee Intermediates Drive Autoxidation in Unsaturated Lipids. *Proc. Natl. Acad. Sci. U. S. A.* **2020**, *117*, 4486–4490.
(21) Popolan-Vaida, D. M.; Wilson, K. R.; Leone, S. R. Reaction of Iodine Atoms with Submicrometer Squalane and Squalene Droplets: Mechanistic Insights into Heterogeneous Reactions. *J. Phys. Chem. A* **2014**, *118*, 10688–10698.
(22) Liu, C.-L.; Smith, J. D.; Che, D. L.; Ahmed, M.; Leone, S. R.; Wilson, K. R. The Direct Observation of Secondary Radical Chain Chemistry in the Heterogeneous Reaction of Chlorine Atoms with Submicron Squalane Droplets. *Phys. Chem. Chem. Phys.* **2011**, *13*, 8993–9007.
(23) Wilson, K. R.; Jimenez-Cruz, M.; Nicolas, C.; Belau, L.; Leone, S. R.; Ahmed, M. Thermal Vaporization of Biological Nanoparticles: Fragment-Free Vacuum Ultraviolet Photoionization Mass Spectra of Tryptophan, Phenylalanine-Glycine-Glycine, and *B*-Carotene. *J. Phys. Chem. A* **2006**, *110*, 2106–2113.
(24) Smith, J. D.; Kroll, J. H.; Cappa, C. D.; Che, D. L.; Liu, C. L.; Ahmed, M.; Leone, S. R.; Worsnop, D. R.; Wilson, K. R. The Heterogeneous Reaction of Hydroxyl Radicals with Sub-Micron Squalane Particles: A Model System for Understanding the Oxidative Aging of Ambient Aerosols. *Atmos. Chem. Phys.* **2009**, *9*, 3209–3222.
(25) Che, D. L.; Smith, J. D.; Leone, S. R.; Ahmed, M.; Wilson, K. R. Quantifying the Reactive Uptake of OH by Organic Aerosols in a Continuous Flow Stirred Tank Reactor. *Phys. Chem. Chem. Phys.* **2009**, *11*, 7885–7895.

(26) Richards-Henderson, N. K.; Goldstein, A. H.; Wilson, K. R. Large Enhancement in the Heterogeneous Oxidation Rate of Organic Aerosols by Hydroxyl Radicals in the Presence of Nitric Oxide. *J. Phys. Chem. Lett.* **2015**, *6*, 4451–4455.
(27) Richards-Henderson, N. K.; Goldstein, A. H.; Wilson, K. R. Sulfur Dioxide Accelerates the Heterogeneous Oxidation Rate of Organic Aerosol by Hydroxyl Radicals. *Environ. Sci. Technol.* **2016**, *50*, 3554–3561.
(28) Nicolaides, N. Skin Lipids: Their Biochemical Uniqueness. *Science* **1974**, *186*, 19–26.
(29) Ezell, M. J.; Wang, W.; Ezell, A. A.; Soskin, G.; Finlayson-Pitts, B. J. Kinetics of Reactions of Chlorine Atoms with a Series of Alkenes at 1 Atm and 298 K: Structure and Reactivity. *Phys. Chem. Chem. Phys.* **2002**, *4*, 5813–5820.
(30) Bennett, J. E.; Summers, R. Product Studies of the Mutual Termination Reactions of Sec-Alkylperoxy Radicals: Evidence for Non-Cyclic Termination. *Can. J. Chem.* **1974**, *52*, 1377–1379.
(31) Russell, G. A. Deuterium-Isotope Effects in the Autoxidation of Aralkyl Hydrocarbons. Mechanism of the Interaction of Peroxy Radicals[1]. *J. Am. Chem. Soc.* **1957**, *79*, 3871–3877.
(32) Vijayakumar, S.; Rajakumar, B. Theoretical Investigations on the Kinetics of Cl Atom Initiated Reactions of Series of 1-Alkenes. *Environ. Sci. Pollut. Res. Int.* **2018**, *25*, 4387–4405.
(33) Gupta, P.; Rajakumar, B. Reaction Kinetics of a Series of Alkenes with ClO and BrO Radicals: A Theoretical Study. *Int. J. Chem. Kinet.* **2021**, *53*, 250–264.
(34) Beichert, P.; Wingen, L.; Lee, J.; Vogt, R.; Ezell, M. J.; Ragains, M.; Neavyn, R.; Finlayson-Pitts, B. J. Rate Constants for the Reactions of Chlorine Atoms with Some Simple Alkanes at 298 K: Measurement of a Self-Consistent Set Using Both Absolute and Relative Rate Methods. *J. Phys. Chem. A* **1995**, *99*, 13156–13162.
(35) Pekkanen, T. T.; Arppe, S. L.; Eskola, A. J.; Rissanen, M. P.; Timonen, R. S. An Experimental Study of the Kinetics of the Reactions of Isopropyl, Sec-Butyl, Andtert-Butyl Radicals with Molecular Chlorine at Low Pressures (0.5-7.0 Torr) in the Temperature Range 190-480 K. *Int. J. Chem. Kinet.* **2016**, *48*, 796–805.
(36) Vasenkov, S. V.; Bagryansky, V. A.; Korolev, V. V.; Tolkatchev, V. A. Correlations between Radical Distributions and Structural Defects of Squalane and Poly(Methyl Methacrylate) Glasses in the Oxidation Kinetics of Radicals. *Radiat. Phys. Chem.* **1991**, *38*, 191–197.
(37) Young, C. L. *Sulfur Dioxide, Chlorine, Fluorine and Chlorine Oxides: Solubility Data Series*; Pergamon Press: Oxford, 1983; Vol. 12.
(38) Gord, J. R.; Zhao, X.; Liu, E.; Bertram, T. H.; Nathanson, G. M. Control of Interfacial Cl_2 and N_2O_5 Reactivity by a Zwitterionic Phospholipid in Comparison with Ionic and Uncharged Surfactants. *J. Phys. Chem. A* **2018**, *122*, 6593–6604.
(39) Villano, S. M.; Huynh, L. K.; Carstensen, H.-H.; Dean, A. M. High-Pressure Rate Rules for Alkyl + O_2 Reactions. 1. The Dissociation, Concerted Elimination, and Isomerization Channels of the Alkyl Peroxy Radical. *J. Phys. Chem. A* **2011**, *115*, 13425–13442.
(40) Atkinson, R.; Baulch, D. L.; Cox, R. A.; Hampson, R. F.; Kerr, J. A.; Rossi, M. J.; Troe, J. Evaluated Kinetic, Photochemical and Heterogeneous Data for Atmospheric Chemistry: Supplement V. Iupac Subcommittee on Gas Kinetic Data Evaluation for Atmospheric Chemistry. *J. Phys. Chem. Ref. Data* **1997**, *26*, 521–1011.
(41) Kumar, M.; Trabelsi, T.; Gomez Martin, J. C.; Saiz-Lopez, A.; Francisco, J. S. HIO_x-$IONO_2$ Dynamics at the Air-Water Interface: Revealing the Existence of a Halogen Bond at the Atmospheric Aerosol Surface. *J. Am. Chem. Soc.* **2020**, *142*, 12467–12477.

TOC Graphic

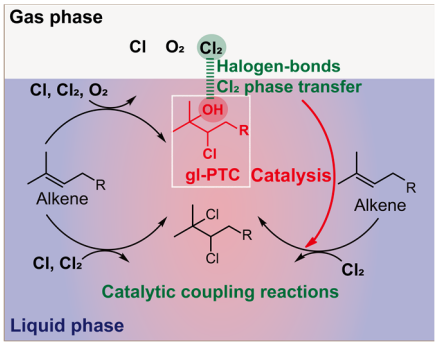
Gas phase
Cl
O₂
Cl₂
Halogen-bonds
Cl₂ phase transfer
Cl, Cl₂, O₂
OH
R
Cl
gl-PTC
Catalysis
Alkene
R
Alkene
R
Cl
R
Cl
Cl, Cl₂
Cl₂
Catalytic coupling reactions
Liquid phase

Supporting Information for

Catalytic Coupling of Free Radical Oxidation and Electrophilic Chlorine Addition by Phase-transfer Intermediates in Liquid Aerosols

Authors: Meirong Zeng,[1,#] Chen-Lin Liu,[2] Kevin R. Wilson[1,*]

Affiliations: [1]Chemical Sciences Division, Lawrence Berkeley National Laboratory, Berkeley, CA 94720, USA. [2]Scientific Research Division, National Synchrotron Radiation Research Center, Hsinchu 30076, Taiwan

[#] Current Address: College of Smart Energy, Shanghai Jiao Tong University, Shanghai, 200240

***Corresponding author**: Kevin R. Wilson (email: krwilson@lbl.gov, Phone: 510-495-2474)

ORCID: Kevin R. Wilson, 0000-0003-0264-0872

Meirong Zeng, 0000-0003-3902-7430

This file contains:

- **Table S1.** The formulas and *m/z* of reactants and products discussed in this work.
- **Section S1.** Reference observations for Sqe + Cl_2 + gl-PTC additives reactions
- **Section S2**. Reference observations for Sqa (no C=C) + Cl_2 + Cl atom
- **Section S3**. Additional experiments for Sqe (6 C=C) + Cl_2 + Cl atom
- **Section S4**. Additional experiments for LNA (3 C=C) + Cl_2 + Cl atom
- **Section S5**. Additional experiments for OA (1 C=C) + Cl_2 + Cl atom

■ ***Table S1.*** Molecular formulas of the reactants and products and the corresponding ions (m/z and loss channels) used to assign the peaks in the experimental mass spectra.

Neutral species (formulas)	loss	Detected ion (formulas, *m/z*)	Neutral species (formulas)	loss	Detected ion (*m/z*)
Squalene (Sqe) reaction system			Linolenic acid (LNA) reaction system		
Sqe ($C_{30}H_{50}$)	N/A	Sqe ($C_{30}H_{50}^+$, 410)	LNA ($C_{18}H_{30}O_2$)	N/A	LNA ($C_{18}H_{30}O_2^+$, 278)
$SqeCl_2$ ($C_{30}H_{50}Cl_2$)	–2 HCl	Sqe-2 ($C_{30}H_{48}^+$, 408)	$LNACl_2$ ($C_{18}H_{30}Cl_2O_2$)	–2 HCl	LNA-2 ($C_{18}H_{28}O_2^+$, 276)
$SqeCl_2$ ($C_{30}H_{50}Cl_2$)	–1 HCl	SqeCl ($C_{30}H_{49}Cl^+$, 444)	$LNACl_2$ ($C_{18}H_{30}Cl_2O_2$)	–1 HCl	LNACl ($C_{18}H_{29}O_2Cl^+$, 312)
$SqeCl_4$ ($C_{30}H_{50}Cl_4$)	–3 HCl	SqeCl ($C_{30}H_{47}Cl^+$, 442)	$LNACl_2$ ($C_{18}H_{30}Cl_2O_2$)	N/A	$LNACl_2$ ($C_{18}H_{30}O_2Cl_2^+$, 348)
$SqeCl_2$ ($C_{30}H_{50}Cl_2$)	N/A	$SqeCl_2$ ($C_{30}H_{50}Cl_2^+$, 480)	LNAO ($C_{18}H_{30}O_3$)	N/A	LNAO ($C_{18}H_{30}O_3^+$, 294)
$SqeCl_4$ ($C_{30}H_{50}Cl_4$)	–2 HCl	$SqeCl_2$ ($C_{30}H_{48}Cl_2^+$, 478)	LNAO ($C_{18}H_{28}O_3$)	N/A	LNAO ($C_{18}H_{28}O_3^+$, 292)
SqeClO ($C_{30}H_{51}ClO$)	–1 HCl	SqeO ($C_{30}H_{50}O^+$, 426)	Oleic acid (OA) reaction system		
SqeClO ($C_{30}H_{49}ClO$)	–1 HCl	SqeO ($C_{30}H_{48}O^+$, 424)	OA ($C_{18}H_{34}O_2$)	N/A	OA ($C_{18}H_{34}O_2^+$, 282)
$C_{27}O$ ($C_{27}H_{44}O$)	N/A	$C_{27}O$ ($C_{27}H_{44}O^+$, 384)	OAO ($C_{18}H_{34}O_3$)	N/A	OAO ($C_{18}H_{34}O_3^+$, 298)
$C_{22}O$ ($C_{22}H_{36}O$)	N/A	$C_{22}O$ ($C_{22}H_{36}O^+$, 316)	OAO ($C_{18}H_{32}O_3$)	N/A	OAO ($C_{18}H_{32}O_3^+$, 296)
$C_{17}O$ ($C_{17}H_{28}O$)	N/A	$C_{17}O$ ($C_{17}H_{28}O^+$, 248)	$OACl_2$ ($C_{18}H_{34}Cl_2O_2$)	–2 HCl	OA-2 ($C_{18}H_{32}O_2^+$, 280)
			$OACl_2$ ($C_{18}H_{34}Cl_2O_2$)	–1 HCl	OACl ($C_{18}H_{33}O_2Cl^+$, 316)
Squalane (Sqa) reaction system					
Sqa ($C_{30}H_{62}$)	N/A	Sqa ($C_{30}H_{62}^+$, 422)	SqaO ($C_{30}H_{62}O$)	N/A	SqaO ($C_{30}H_{62}O^+$, 438)
SqaCl ($C_{30}H_{61}Cl$)	–1 HCl	Sqa-2 ($C_{30}H_{60}^+$, 420)	SqaO ($C_{30}H_{60}O$)	N/A	SqaO ($C_{30}H_{60}O^+$, 436)
$SqaCl_2$ ($C_{30}H_{60}Cl_2$)	–1 HCl	SqaCl ($C_{30}H_{59}Cl^+$, 454)	$SqaCl_3$ ($C_{30}H_{59}Cl_3$)	–1 HCl	$SqaCl_2$ ($C_{30}H_{58}Cl_2^+$, 488)

■ *S1. Reference observations for Sqe + Cl_2 + gl-PTC additives reactions*

In a previous study we examined the heterogeneous electrophilic addition of Cl_2 to Sqe. We observed that the presence of oxygenated additives were effective gas-liquid phase transfer catalysts (gl-PTC)[1]. Three oxygenated additives, 2-decyl-1-tetradecanol ($C_{24}OH$), linoleic acid

(LA) and oleic acid (OA), are mixed into a Sqe aerosol to form a binary mixture, *e.g.* Sqe + $C_{24}OH$. γ_{eff} for Sqe was observed to increase significantly in the presence of the additives (Fig. S1B). It was hypothesized[1] that the formation of interfacial halogen-bonds to the oxygenated functional group of the additive (*i.e.* –OH, and –COOH groups) enhanced the accommodation of Cl_2 gas in the Sqe aerosol. This enhanced gas capture accelerated the electrophilic addition of Cl_2 to Sqe evidenced by an increase in γ_{eff}.

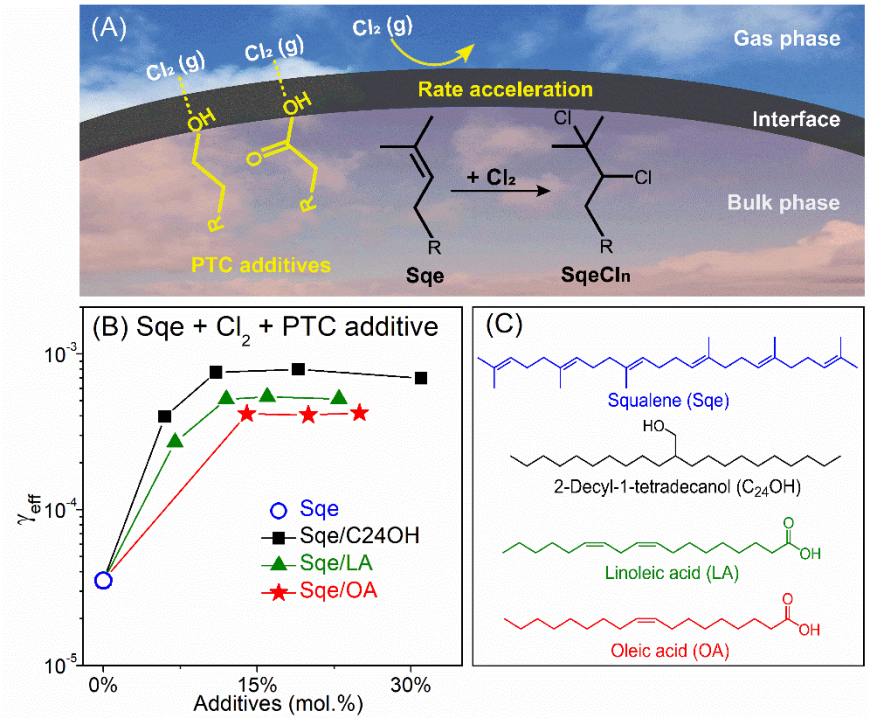

Fig. S1. Figure reproduced from the Ref.[1] with permission from the Royal Society of Chemistry. (A) Proposed mechanism for enhanced electrophilic addition of Cl_2 to Sqe + Cl_2 in the presence of $C_{24}OH$, LA and OA additives, which act as gl-PTC. (B) γ_{eff} of Sqe as a function of additive mole fractions. (C) Chemical structures of Sqe and the three gl-PTC additives.

■ *S2. Reference observations for Sqa (no C=C) + Cl_2 + Cl atom*

The reaction of Cl atoms with Sqa (a $C_{30}H_{62}$ branched alkane without C=C bonds) in the presence of O_2 and Cl_2 was investigated previously[2]. In the absence of O_2, chlorinated products (denoted Sqa-2 and $SqaCl_n$) are major species produced in the reaction. In contrast oxygenated products (denoted SqaO) appear in the presence of O_2, as reproduced in Fig. S2. Figure S3 shows an abbreviated mechanism for the Sqa + Cl (with Cl_2) reaction[2]. The reaction begins upon H-abstraction by Cl atoms and is propagated by alkyl radical reactions with Cl_2 to generate Cl atoms and chlorinated products (*e.g.* $SqaCl_n$). In the presence of O_2, the mechanism shifts to the canonical free radical oxidation pathway involving chain terminating peroxy radical reactions that produce ketones and alcohols (*e.g.* SqaO). Both chlorinated products and oxygenates were detected as

shown in Fig. S2, which provides direct evidence for both sub-mechanisms that are shown in Fig. S3.

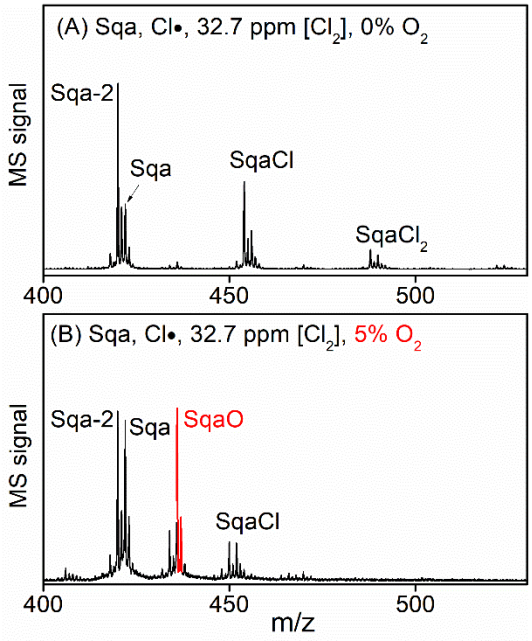

Fig. S2. VUV-AMS mass spectra recorded for the Sqa + Cl (with Cl_2) reaction: (A) without O_2 and (B) with 5% O_2 showing the major chlorinated ($SqaCl_n$) and oxygenated (SqaO) products. Figure reproduced from Ref.[2] with permission of the Royal Society of Chemistry.

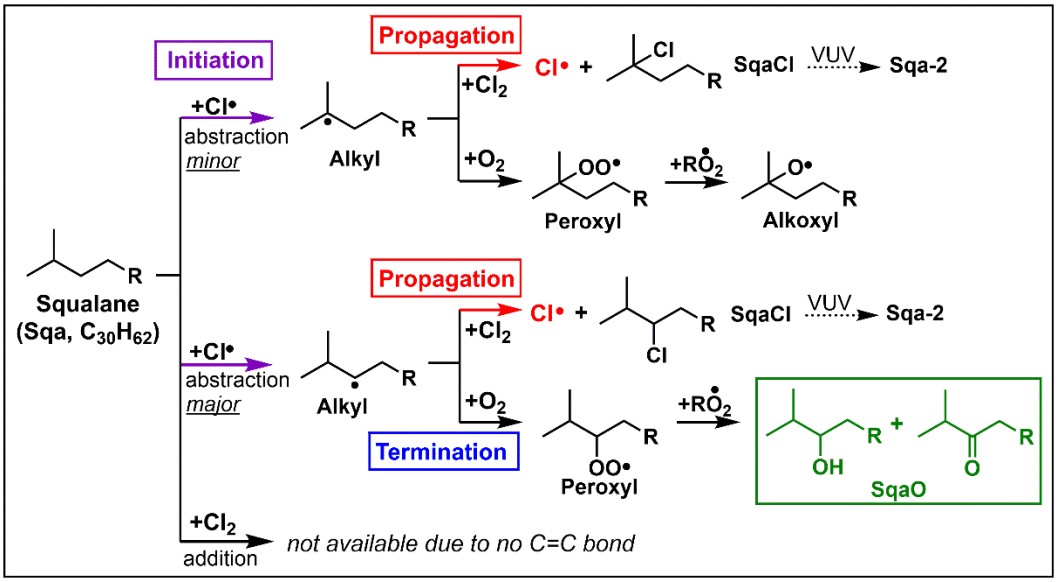

Fig. S3. Abbreviated mechanism for the Sqa + Cl_2 + Cl reaction from Ref.[2]. The scheme includes two sub-mechanisms: (1) chlorine atom reactions involving Cl_2 and (2) free radical oxidation chemistry.

■ *S3. Additional experiments for Sqe (6 C=C) + Cl_2 + Cl atom*

Experiments are conducted by fixing the [Cl_2] in the flow tube reactor and first measuring the amount of Sqe decay in the dark (*i.e.* no Cl atoms). Figure S4 shows the decay of Sqe, due to electrophilic Cl_2 addition, as a function of [Cl_2]. The UV lights are then turned on to initiate the Cl atom reactions. For each flow tube experiment with fixed [Cl_2], the decay kinetics of Sqe is measured as a function of [Cl] exposure by changing the photon flux of the UV lamps. The decay kinetics (with the lights on) is then used to compute γ_{eff} as shown in Figs. S5 and S8. Figures S7 and S9 show decay kinetics measured in the CFSTR.

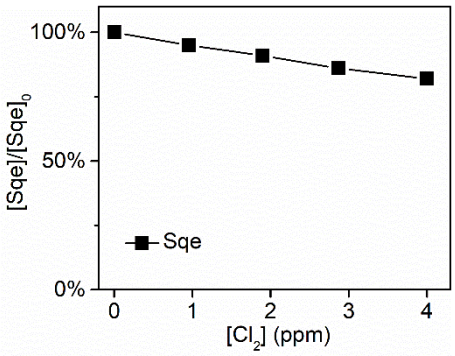

Fig. S4. The fraction of Sqe consumed as a function of [Cl_2], in the dark, arising from Sqe + Cl_2 reaction (no Cl atoms). Experiments (symbols) are conducted in the flow tube reactor.

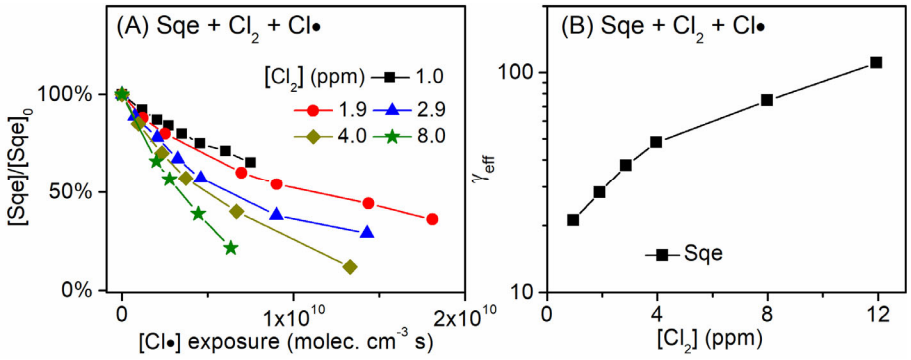

Fig. S5. (A) Decay kinetics of Sqe as a function of Cl atom exposure in the absence of O_2. (B) γ_{eff} as a function of [Cl_2]. Experiments (symbols) are conducted in the flow tube reactor.

Figure S6 presents the reaction scheme and product analysis for Sqe + Cl/Cl_2 reaction *without* O_2. It includes three main sub-mechanisms: (1) Cl atom reactions, (2) free radical oxidation, and (3) electrophilic Cl_2 addition. The Cl + Sqe reaction produces a chlorinated alkyl radical (R·) and is propagated by the R· + Cl_2 reaction to generate Cl atoms and chlorinated products ($SqeCl_n$). The

free radical oxidation chemistry is similarly initiated, generating a chlorinated R·, which reacts with O_2 to form a chlorinated peroxy radicals (RO_2·). RO_2· + RO_2· reactions[3-5] produce oxygenated products (*i.e.* gl-PTC). Electrophilic addition of Cl_2 to the C=C bond(s) of Sqe and its products (*e.g.* $SqeCl_2$) produce a series of chlorinated species ($SqeCl_n$) at each of the 6 C=C bonds locations in Sqe.

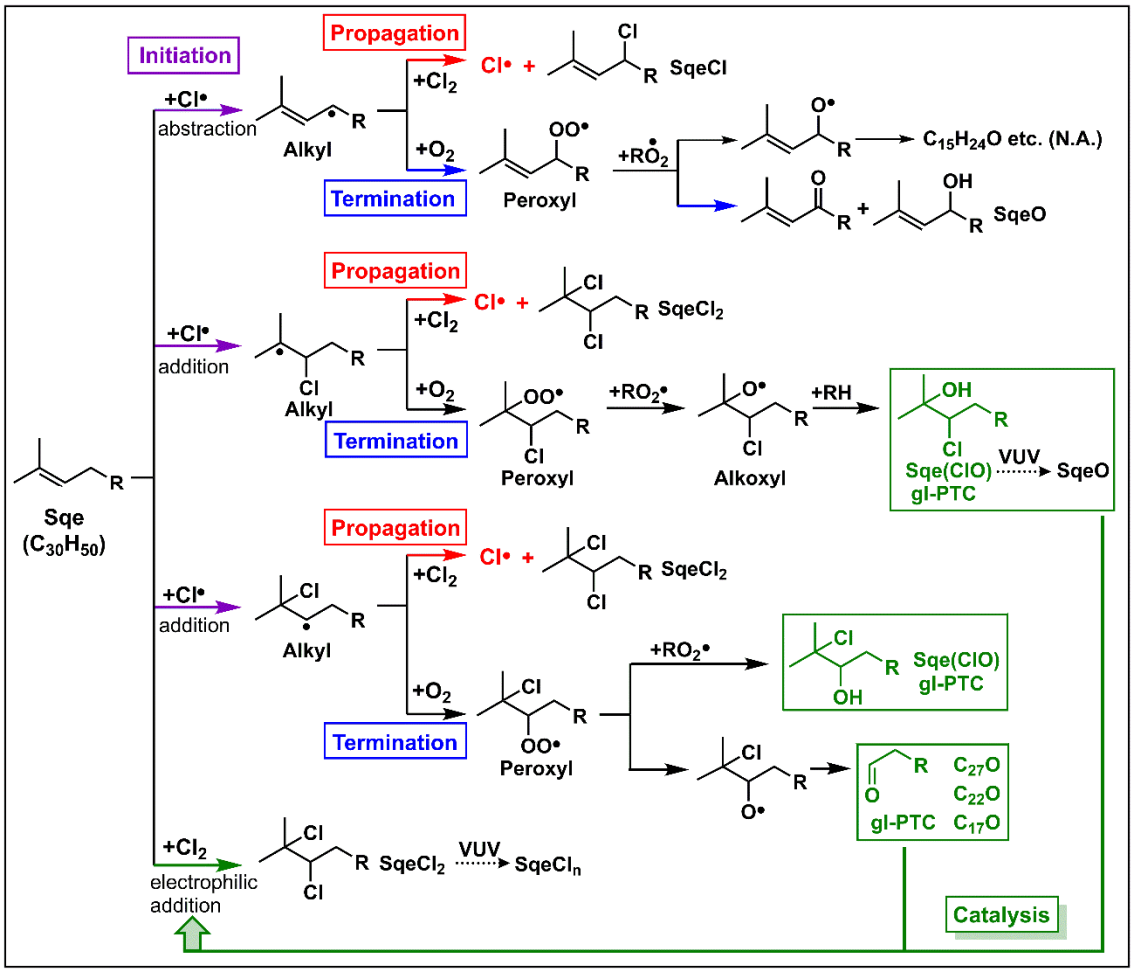

Fig. S6. Abbreviated scheme showing the major pathways and products for Sqe + $Cl/Cl_2/O_2$ reaction. The scheme includes three sub-mechanisms, *i.e.* the chlorine atom/Cl_2 chemistry, free radical oxidation, and electrophilic Cl_2 addition. The pathways are labeled to show initiation, propagation, termination, and catalysis.

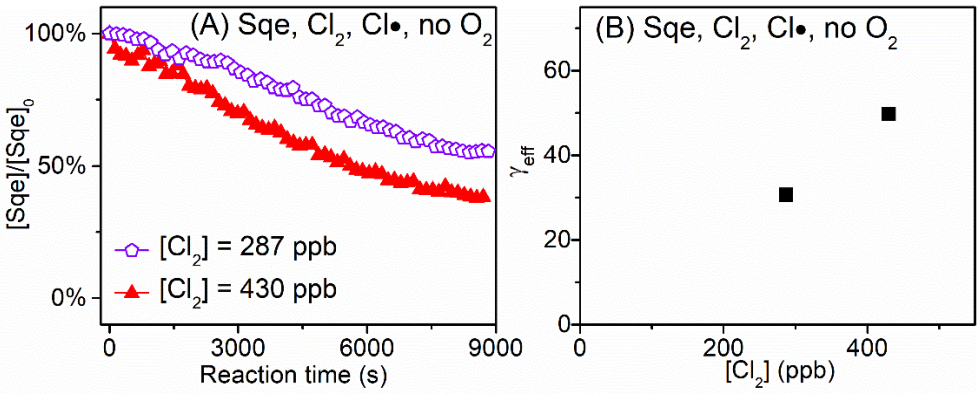

Fig. S7. (A) The decay kinetics of Sqe during the Sqe + Cl_2 + Cl reaction (without O_2), (B) γ_{eff} as a function of [Cl_2] measured in the CFSTR.

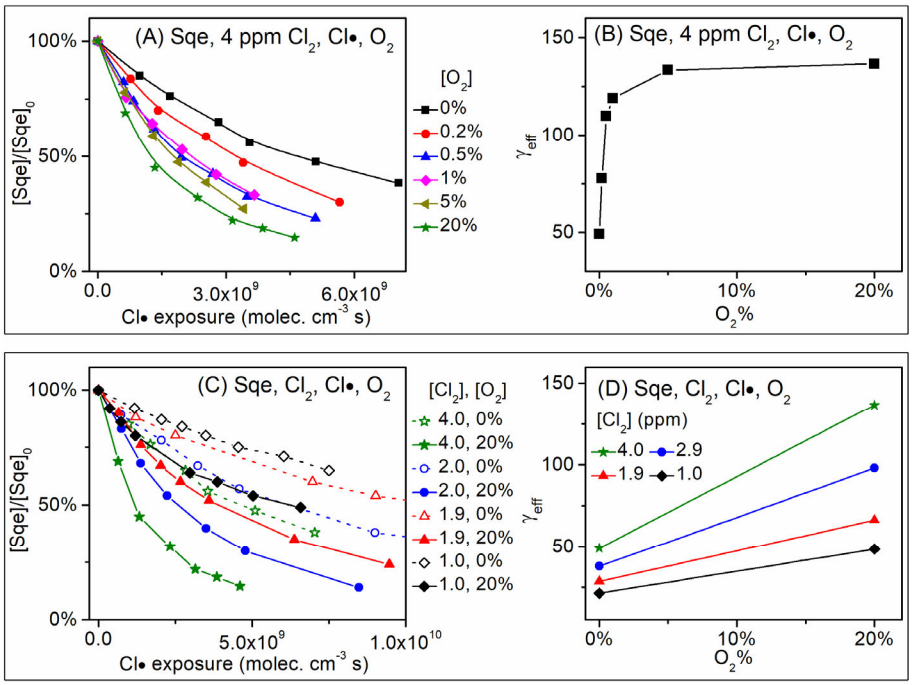

Fig. S8. (A and C) The decay kinetics of Sqe as a function of Cl atom exposure, [O_2] and [Cl_2], (B and D) γ_{eff} as a function of [O_2] and [Cl_2] measured in the flow tube reactor.

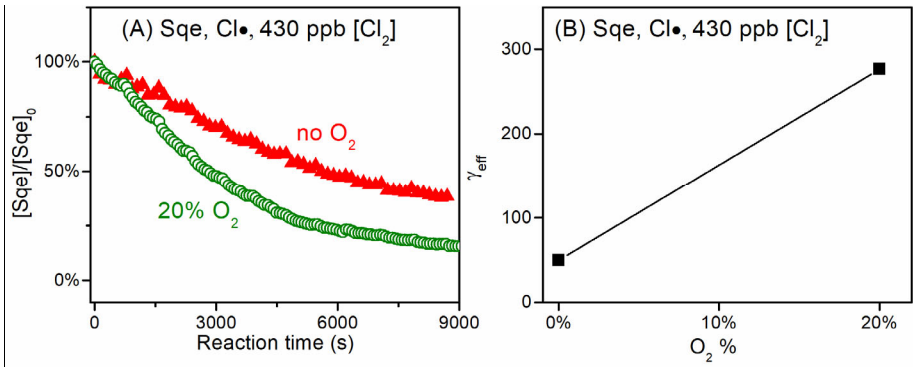

Fig. S9. (A) The decay of Sqe as a function of reaction time, (B) γ_{eff} of Sqe as a function of [O_2] during the Sqe + Cl_2 + Cl atom *w/o* O_2 reactions in the CFSTR.

■ *S4. Additional experiments for LNA (3 C=C) + Cl_2 + Cl atom*

This section includes additional experiments and mechanisms for the heterogeneous reaction of linolenic acid (LNA, with 3 C=C bonds) as a function of [Cl], [Cl_2] and [O_2]. Figure S10 shows difference mass spectra, which shows chlorinated (denoted LNA-2 and $LNACl_n$) at 0% O_2 and oxygenated products (named as LNAO) at 20% O_2. Figure S11 shows the increased γ_{eff} of LNA as a function of [O_2], which is consistent with what is observed for Sqe (*e.g.* Fig. 1B).

Figure S12 illustrates reaction scheme and product analysis for the LNA reaction, which is similar to that for Sqe described in main text and *Section S2.* The LNA reaction includes three sub-mechanisms described above for Sqe that illustrate how chlorinated products (*e.g.* $LNACl_n$) are formed as well as the free radical oxidation pathways that produce oxygenates (*e.g.* LNA(ClO)). Electrophilic addition of Cl_2 to LNA is also shown. The chlorinated and oxygenated products produced by these pathways are mostly detected as fragments in the VUV photoionization mass spectra. These fragmentation pathways are shown with dashed arrows in Fig. S12.

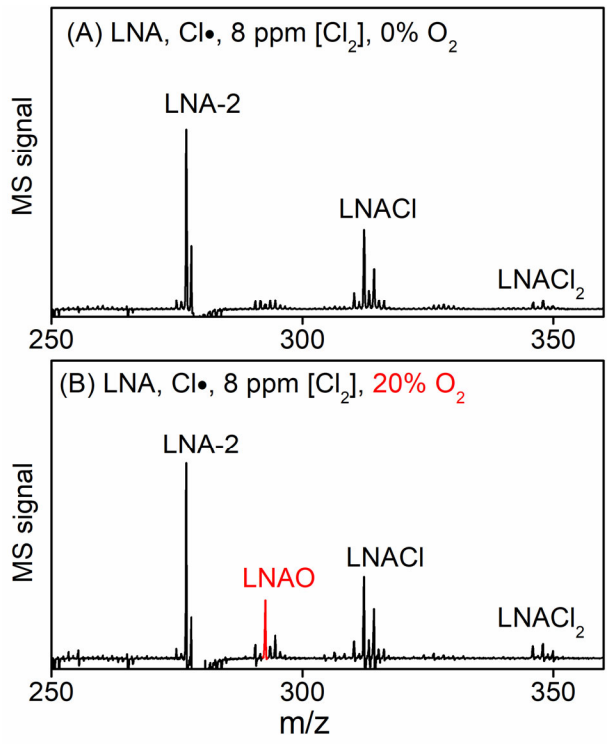

Fig. S10. Difference VUV-AMS mass spectra of LNA + Cl_2 + Cl: (A) without O_2 and (B) with 20% O_2. Chlorinated products (LNA-2, $LNACl_n$) are major products in (A) while, oxygenated products (*e.g.* LNAO) appear at 20% O_2. Experiments are conducted in the flow tube reactor.

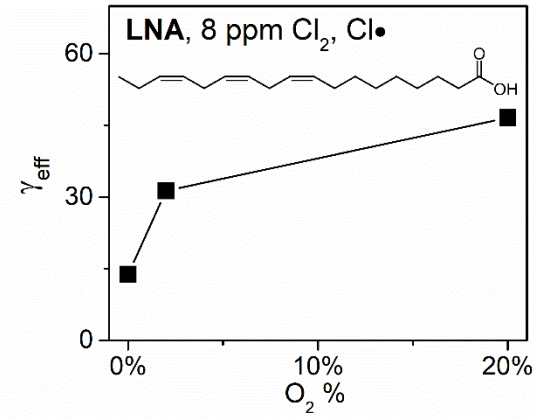

Fig. S11. γ_{eff} as a function of O_2 for the LNA reaction conducted in the flow tube reactor.

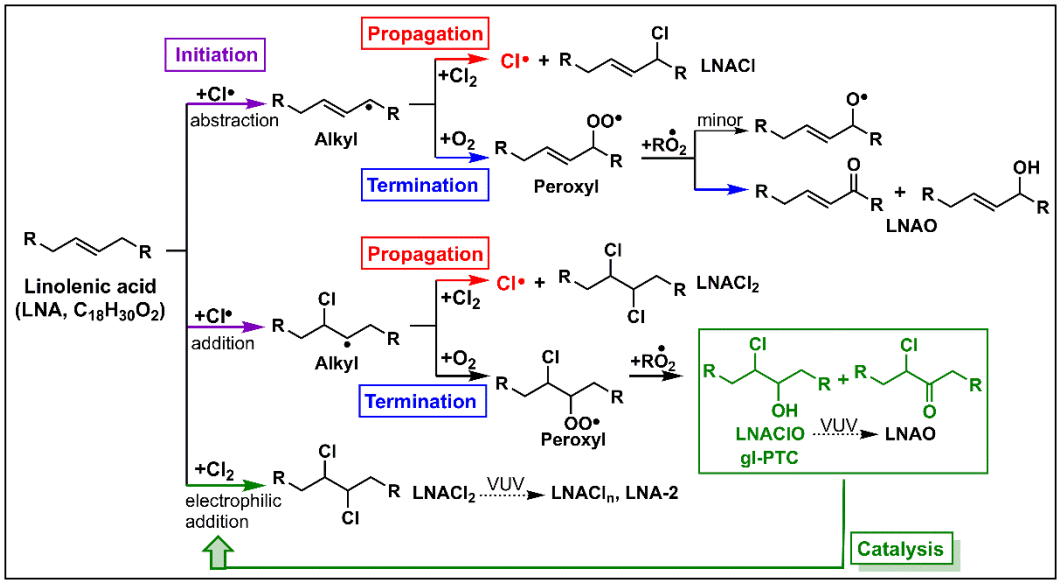

Fig. S12. Reaction scheme and product analysis for LNA system. The abbreviated scheme includes three sub-mechanisms, (1) Cl atom/Cl_2 reaction pathways, (2) free radical oxidation and (3) electrophilic addition pathways for Cl_2. Initiation, propagation, termination, and catalysis branches are labeled.

■ *S5. Additional experiments for OA (1 C=C) + Cl_2 + Cl atom*

This section includes additional experiments and catalytic coupling mechanisms for the heterogeneous reaction of oleic acid (OA) aerosol. Figure S13 shows that chlorinated products (*e.g.* OA-2, OACl) are the major products in the absence of O_2, while oxygenates (OAO) appear when introducing O_2. Figure 14 shows the increase in γ_{eff} as a function of [O_2], which is consistent with the dependence observed for both the Sqe and LNA systems described above. Figure S15 illustrates the reaction scheme and product analysis for OA system.

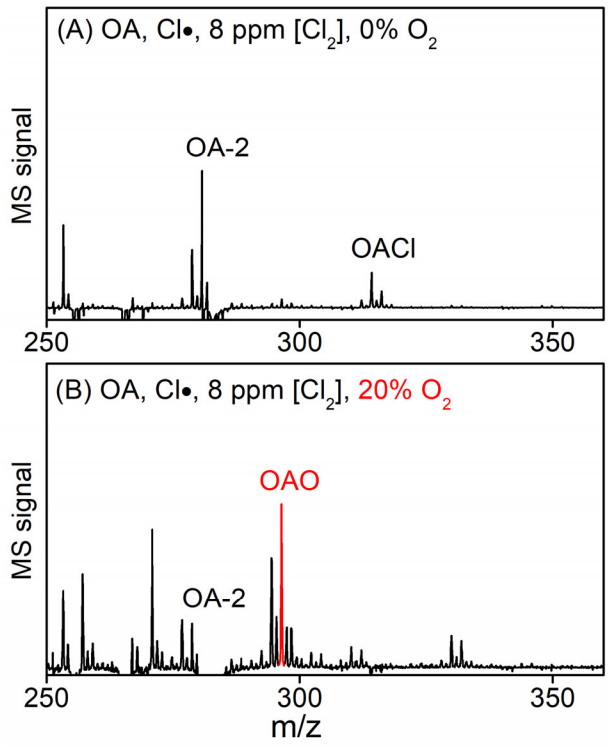

Fig. S13. Difference VUV-AMS mass spectra of OA reaction: (A) without O_2 and (B) with O_2. Chlorinated products ($OACl_n$) are major products in (A), while oxygenated product (OAO) are observed in (B) when $[O_2]$ = 20%.

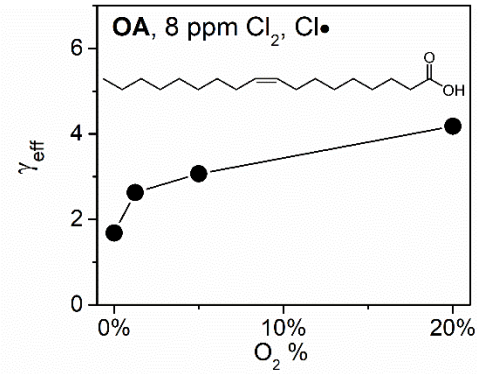

Fig. S14. γ_{eff} function of O_2 for OA obtained in the flow tube reactor.

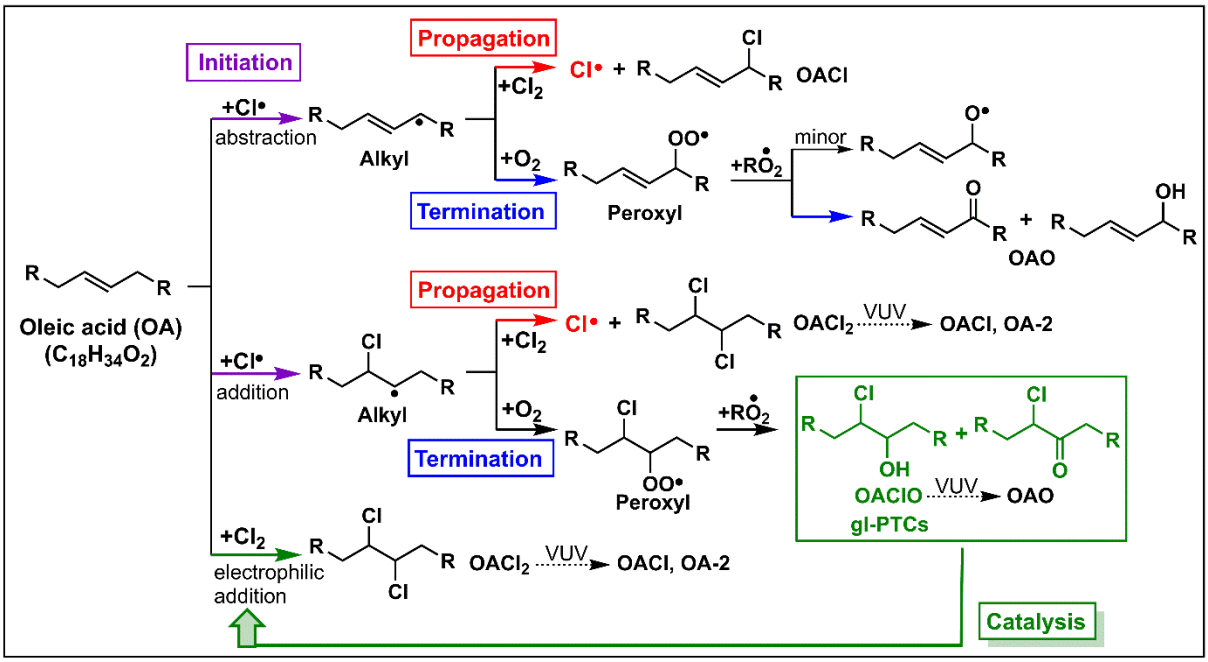

Fig. S15. Reaction scheme and product analysis for OA system. Three sub-mechanisms are show and illustrate chlorine radical/Cl_2, free radical oxidation, and the electrophilic addition pathways.

References.

(1) Zeng, M.; Wilson, K. R. Experimental Evidence That Halogen Bonding Catalyzes the Heterogeneous Chlorination of Alkenes in Submicron Liquid Droplets. *Chem. Sci.* **2021**, *12*, 10455–10466.

(2) Liu, C.-L.; Smith, J. D.; Che, D. L.; Ahmed, M.; Leone, S. R.; Wilson, K. R. The Direct Observation of Secondary Radical Chain Chemistry in the Heterogeneous Reaction of Chlorine Atoms with Submicron Squalane Droplets. *Phys. Chem. Chem. Phys.* **2011**, *13*, 8993–9007.

(3) Bennett, J. E.; Summers, R. Product Studies of the Mutual Termination Reactions of Sec-Alkylperoxy Radicals: Evidence for Non-Cyclic Termination. *Can. J. Chem.* **1974**, *52*, 1377–1379.

(4) Russell, G. A. Deuterium-Isotope Effects in the Autoxidation of Aralkyl Hydrocarbons. Mechanism of the Interaction of Peroxy Radicals[1]. *J. Am. Chem. Soc.* **1957**, *79*, 3871–3877.

(5) Wiegel, A. A.; Wilson, K. R.; Hinsberg, W. D.; Houle, F. A. Stochastic Methods for Aerosol Chemistry: A Compact Molecular Description of Functionalization and Fragmentation in the Heterogeneous Oxidation of Squalane Aerosol by OH Radicals. *Phys. Chem. Chem. Phys.* **2015**, *17*, 4398-411.